

# Analysis of amplified spontaneous emission in ring-core Tm<sup>3+</sup>-doped optical fiber

Krzysztof Markowski\*, Piotr Miluski

<sup>1</sup>Faculty of Electrical Engineering, Bialystok University of Technology, Wiejska 45D, 15-351 Bialystok,

Received December 15, 2023; accepted December 28, 2023; published December 31, 2023

**Abstract**—This paper presents the results of numerical simulations of a ring-core thulium-doped silica fiber (RC-TDF). Enhanced spontaneous emission (ASE) was generated for a fiber with 4wt.% thulium content. An analysis of the formation of the ASE spectrum parameters ( $\lambda_{\max}$ , FWHM, output power) as a function of fiber length is also shown. The modal map is presented as a combination of outer and inner core radii and  $\Delta n$ .

Optical fibers doped with Tm<sup>3+</sup> ions with emission in the eye-safe spectral range are successfully used in amplified spontaneous emission (ASE) radiation sources and fiber lasers [1]. The emission band of thulium ions around 1.8  $\mu\text{m}$  is used in various applications such as telecommunications, medicine, materials processing, LIDAR systems, environmental pollution, and gas detection [2–4]. One of the advantages of using a thulium dopant is the possibility of pumping (excitation) with commonly available laser diodes around 800 nm, using the  $^3\text{H}_6 \rightarrow ^3\text{H}_4$  transition. Thulium-doped silica glass emits radiation in the range of 1600 to 2200 nm, so it can be used to construct broadband ASE sources. Moreover, it is possible to achieve high-efficiency emission using the phenomenon of cross-relaxation between the thulium energy levels  $^3\text{H}_4, ^3\text{H}_6 \rightarrow ^3\text{F}_4, ^3\text{F}_4$  (one-for-two energy transfer) [5]. This phenomenon can be achieved by using a high concentration of Tm<sup>3+</sup> ions (typically above 3.5 wt.% Tm<sub>2</sub>O<sub>3</sub>), increasing the slope efficiency and output power of fiber lasers [6]. On the other hand, it may cause thermal loads in the fiber core, leading to damage or photodarkening. As a compromise, ring-core fibers (RCFs) doped with rare-earth (RE) elements are being developed whose ring doping profile reduces the overlap of propagation modes in the doping region, thereby lowering thermal loads while allowing the use of high concentrations of RE-dopants [7–8].

RCFs supporting a few-mode propagation are used in telecommunications to increase transmission capacity through mode division multiplexing (MDM). It has been proven that optical amplifiers in the MDM system using a few-mode ring-core erbium-doped fiber (RC-EDF) are characterized by a better noise-to-signal ratio, translating into higher signal quality [9]. In addition, there are many

MDM transmission systems using few-mode fibers according to the number of linearly polarized (LP) propagation modes: support two LP modes (LP<sub>01</sub>, LP<sub>11</sub>) [9], three LP modes (LP<sub>01</sub>, LP<sub>11</sub>, LP<sub>21</sub>) [10], and four-LP modes (LP<sub>01</sub>, LP<sub>11</sub>, LP<sub>21</sub>, LP<sub>02</sub>) [11], respectively.

In this paper, we analyze the effect of changing optical fiber construction parameters (fiber length, core geometric size, refractive index) on the spectroscopic properties and propagation characteristics of RC-TDF fiber using numerical simulations. The results may be useful in designing novel few-mode ring-core thulium-doped fiber structures. These have great potential for fiber laser, supercontinuum generation, sensor, and telecommunication applications with emission in an eye-safe spectral range.

The analyzed structure is a silica ring-core thulium-doped optical fiber (RC-TDF), presented in Fig. 1. Numerical simulations were performed to obtain the ASE spectrum and determine the modal properties of the fiber using RP Fiber Power software. The parameters  $R_i$  and  $R_o$  are the inner and outer radii of the core, respectively. The refractive index profile (RIP) base is undoped silica ( $n_{cl} = 1.445$ ), and the  $\Delta n$  parameter determines the difference between the silica base and the doped ring. The inner core and cladding have equal refractive indices, as presented in Fig. 1a.

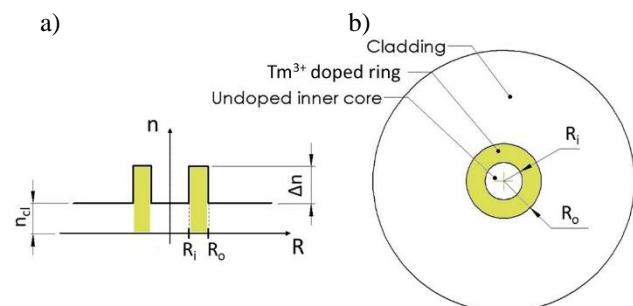


Fig. 1. Diagram of refractive index profile a) and core structure b).

\* E-mail: krzysztof.markowski@sd.pb.edu.pl

The parameters for the ASE spectrum simulation are presented in Table 1, where 4wt.% of thulium dopant was assumed. This dopant concentration supports the phenomenon of one-to-two energy exchange, which is crucial in laser applications. However, a higher dopant concentration is difficult to achieve in the silica host and significantly increases the refractive index. Moreover, a typical construction of silica active fibers contains aluminum, which improves the solubility of rare earth elements and reduces the risk of clustering in this matrix. Therefore, the calculations assumed doping with aluminum according to the Al/Tm molar ratio 10:1 [12]. The  $\Delta n$  parameter was estimated based on the molar content  $c$  of dopants according to the equation [13]:

$$\Delta n = 10^{-4} \cdot [67 \cdot C_{Tm_2O_3} + 22 \cdot C_{Al_2O_3}]. \quad (1)$$

The development of the ASE spectrum (forward and backward) as a function of fiber length was analyzed in the range from 0.1 to 1.0 m. The influence of changing the core parameters (inner and outer radius and refractive index) on the number of linearly polarized (LP) modes was examined. The simulations concern few-mode fibers (up to the first 10 LP modes). Therefore, the outer core radius  $R_o$  range was limited to 10  $\mu\text{m}$ . The calculations were performed for a wavelength of 1800 nm.

Table 1. Parameters for numeric simulations

| Parameter   | Value                |
|---|----------------------|
| $R_i$ range [ $\mu\text{m}$ ]                                 | 1 – 9.5              |
| $R_o$ range [ $\mu\text{m}$ ]                                 | 1.5 – 10             |
| Fiber length range [m]  | 0.1 – 1              |
| Pump power [W]  | 10                   |
| $\lambda_{exc}$ [nm]  | 796                  |
| Ions concentration ( $\text{Tm}^{3+}$ ) [ions/ $\text{m}^3$ ] | $3.33 \cdot 10^{26}$ |

The ASE was simulated at one-end core fiber excitation. The forward CW pump radiation at 796 nm, Gaussian-profile shape, and pulse power 10 W CW was analyzed. The silica/air (c.a. 4%) interface reflections on both optical fiber ends were assumed. The ASE in the forward and backward direction was simulated for 1000 calculation steps per fiber length, 5 nm per channel spectrum. The power spectral density (PSD) of ASE signals in forward and backward directions were investigated in the 1650–2050 nm range. Figure 2 shows the emission spectrum resulting from the  $\text{Tm}^{3+}$ :  $^3F_4 \rightarrow ^3H_6$  transition. The spectrum profile is significantly different in both ASE forming directions. For forward ASE, PSD initially increases with fiber length, reaching a maximum of 0.4 m (0.026 mW/nm) and gradually decreasing. However, for backward ASE, the PSD continuously increases until the end of the studied range. This is related to energy reabsorption by  $\text{Tm}^{3+}$  ions ( $\text{Tm}^{3+}$ :  $^3H_4 \rightarrow ^3H_6$ ), which is especially visible in Fig. 3a.

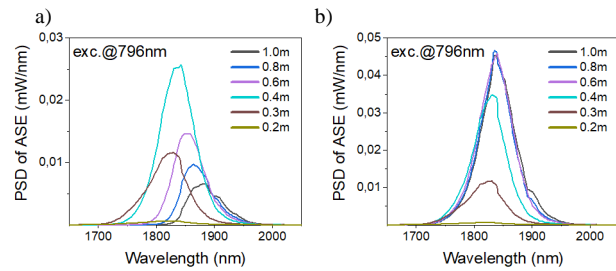


Fig. 2. The ASE spectrum profile for forward a) and backward b) directions.

Numerical calculations indicate that it is possible to modify the ASE spectrum by using the appropriate fiber length (Fig. 3b). The full width at half maximum (FWHM) decreases from 150 to 56 nm for fiber length from 0.1 to 1.0 m. However,  $\lambda_{max}$  shifts slightly towards longer wavelengths (red-shift) from 1819 nm to 1890 nm with the fiber lengths 0.1 m and 1.0 m, respectively.

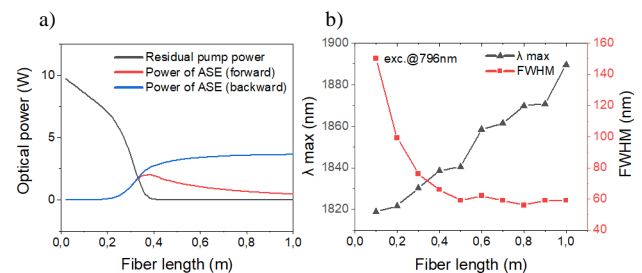


Fig. 3. The variations of the fiber length: output power a), the  $\lambda_{max}$ , and FWHM b) at  $\lambda_{exc} = 796$  nm.

The output power of ASE forward increases as long as it absorbs the pump power. However, then the situation is the opposite of backward ASE. The maximum forward ASE power at the output (2.02 W) occurs for a fiber length of 0.4 m. At the same fiber length, the residual power of the pump is fully absorbed. It is worth mentioning that the method of combined generation of both ends can be used to obtain a more uniform emission profile [14].

Figure 5 shows a map of the modes that can be obtained by combining the radii  $R_i$  and  $R_o$  of the ring core. Simulations were performed with a step of 0.5  $\mu\text{m}$ , for a  $\Delta n = 0.018$  and a wavelength of 1800 nm. This is how individual areas of the same color indicate specific LP modes. Multimode propagation areas dominate the studied range. It is easy to notice that the larger the core radius and the more significant the difference between  $R_i$  and  $R_o$ , the more LP modes occur. It is also worth adding that a larger difference between  $R_i$  and  $R_o$  favors the appearance of  $\text{LP}_{lm}$  modes with index  $m > 1$  (circularly symmetric modes). The fiber we consider in ASE simulations is characterized by the propagation of nine LP modes ( $\text{LP}_{01}$ ,  $\text{LP}_{11}$ ,  $\text{LP}_{21}$ ,  $\text{LP}_{31}$ ,  $\text{LP}_{41}$ ,  $\text{LP}_{51}$ ,  $\text{LP}_{02}$ ,  $\text{LP}_{12}$ ).

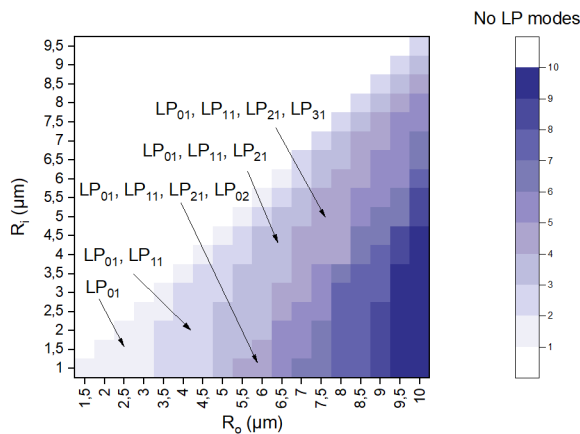


Fig. 5. Map of the allowable LP modes for  $R_i$  and  $R_o$  combinations at 1800 nm,  $\Delta n = 0.018$ .

An analysis of the influence of changing the refractive index  $\Delta n$  (in the range of 0.002–0.018) and the ratio of  $R_i$  and  $R_o$  radii on the number of modes was carried out. The ratio  $d$  was introduced according to the relationship:

$$d = \frac{R_i}{R_o}, \quad (2)$$

where  $R_o$  was assumed to be a constant value of 10  $\mu\text{m}$ .

As Fig. 6 shows, the number of supported LP modes increases as the refractive index increases. Dual-mode propagation ( $\text{LP}_{01}$ ,  $\text{LP}_{11}$ ) is only available for  $\Delta n < 0.006$  for the considered values of the  $d$  parameter. This may be an exciting area for fibers with a large mode area (LMA), which is characterized by a low numerical aperture value ( $\text{NA} < 0.06$ ) [15]. However, low numerical aperture causes high bending sensitivity. It has been proven that few-mode ring-core fibers have exceptional resistance to bending compared to classic step-index structures [16], which is crucial in applications where operational stability is essential. It should also be noted that increasing the thickness of the core ring causes a proportional increase in the number of modes.

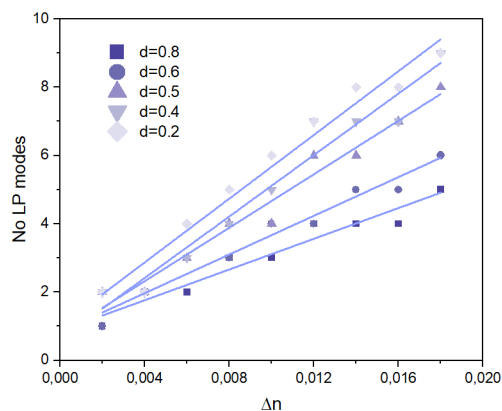


Fig. 6. Number of the allowable LP modes for  $\Delta n$  and  $d$  variations at 1800 nm,  $R_o = 10 \mu\text{m}$ .

In this article, we analyzed a few-mode ring-core thulium-doped fiber. The ASE numerical simulations confirmed the possibility of profiling the emission spectrum by changing the fiber length. The FWHM of the emission profile decreased from 150 to 56 nm for fiber length from 0.1 to 1.0 m, respectively, and the spectrum shifted towards longer waves. Analyzing fiber length variations also allows for estimating the optimal fiber length for maximum power generation. The total pump power was absorbed for a fiber length of 0.4 m, while the ASE forward power reached the maximum. Combining the inner and outer core radii, the developed mode map showed that propagation from 2-mode ( $\text{LP}_{01}$ ,  $\text{LP}_{11}$ ) to 9-mode is possible in the entire tested range. The analysis showed that a larger ring thickness increases the number of modes and increases the probability of the appearance of circularly symmetric modes ( $m > 1$ ). The presented results can be used to design new radiation sources operating in the eye-safe spectral range.

This work was funded by Bialystok University of Technology no. WI/WE-IA/10/2023.

## References

- [1] Y. Huang, Q. Xu, S. Peng, C. Xu, T. Liao, *Opt. Laser. Technol.* **153**, 108282 (2022).
- [2] D. Theisen-Kunde, V. Ott, R. Brinkmann, R. Keller, *Medical Laser Application* **22**, 139 (2007).
- [3] N.P. Barnes, B.M. Walsh, D.J. Reichle, R.J. DeYoung, *Opt. Mater. (Amst.)* **31**, 1061 (2009).
- [4] S.W. Henderson, C.P. Hale, J.R. Magee, M.J. Kavaya, A.V. Huffaker, *Opt. Lett.* **16**, 773 (1991).
- [5] S.D. Jackson, *Opt. Comm.* **230**, 197 (2004).
- [6] J. Wu, S. Jiang, T. Luo, J. Geng, N. Peyghambarian, N.P. Barnes, *IEEE Photon. Technol. Lett.* **18**, 334 (2006).
- [7] M. J. Barber, P. C. Shardlow, P. Barua, J. K. Sahu, W. A. Clarkson, *Opt. Lett.* **45**, 5542 (2020).
- [8] P. Miluski, K. Markowski, M. Kochanowicz, M. Łodziński, J. Żmojda, W.A. Pisarski, J. Pisarska, M. Kuwik, M. Leśniak, D. Dorosz, T. Ragiń, V. Askirka, J. Dorosz, *Sci Rep.* **13**, 13963 (2023).
- [9] H. Ono, T. Hosokawa, K. Ichii, S. Matsuo, H. Nasu, M. Yamada, *Opt. Expr.* **23**, 27405 (2015).
- [10] M. Kasahara, K. Saitoh, T. Sakamoto, N. Hanzawa, T. Matsui, K. Tsujikawa, F. Yamamoto, *J. Lightwave Techn.* **32**, 1337 (2014).
- [11] P. Sillard, M. Bigot-Astruc, D. Boivin, H. Maerten, L. Provost, *37th European Conference and Exposition on Optical Communications*, OSA, Washington, D.C., p. Tu.5.LeCervin.7 (2011).
- [12] S.D. Jackson, S. Mossman, *Appl. Opt.* **42**, 2702 (2003).
- [13] S. Unger, A. Schwuchow, J. Dellith, J. Kirchhof, *Opt. Mater. Expr.* **10**, 907 (2020).
- [14] P. Honzatko, Y. Baravets, I. Kasik, O. Podrazky, *Opt. Lett.* **39**, 3650 (2014).
- [15] P. Miluski, M. Kochanowicz, J. M. Zmojda, A. Baranowska, M. Leśniak, D. Dorosz, K. Markowski, J. Dorosz, in *Fiber Lasers and Glass Photonics: Materials through Applications III* (Eds.: S. Taccheo, M. Ferrari, A.B. Seddon), SPIE p. 48. (2022)
- [16] Y. Jung, Q. Kang, H. Zhou, R. Zhang, S. Chen, H. Wang, Y. Yang, X. Jin, F. P. Payne, S. Alam, D.J. Richardson, *J. Lightwave Techn.* **35**, 1363 (2017).